Energy & Buildings 296 (2023) 113393

Contents lists available at ScienceDirect

Energy & Buildings

journal homepage: www.elsevier.com/locate/enb

Estimation of thermal resistance and capacitance of a concrete wall from *in situ* measurements: A comparison of steady-state and dynamic models

Beñat Arregi [a,*], Roberto Garay-Martinez [b], Juan Carlos Ramos [c]

[a] TECNALIA, Basque Research and Technology Alliance (BRTA), Derio, Spain
[b] University of Deusto, Institute of Technology, Faculty of Engineering, Bilbao, Spain
[c] Universidad de Navarra, TECNUN Escuela de Ingeniería, San Sebastian, Spain

ARTICLE INFO

Keywords:
Building envelope
In situ measurements
Heat flow meter method
Thermal resistance
Thermal capacitance

ABSTRACT

There is a growing interest in characterising the thermal performance of building envelopes when exposed to realistic weather and indoor conditions. In this study, data from a full-scale test of four uninsulated concrete panels is analysed using (1) a steady-state model as per the standard average method, (2) a dynamic lumped resistance–capacitance model with a stochastic method, and (3) a dynamic distributed capacitance model based on an analytical solution. These have been favoured over purely data-driven methods, since their physical formulation allows the characterisation of thermal capacity alongside the usual thermal resistance. The models are applied to different data subsets, sampling times and campaign lengths. For the sole estimation of thermal resistance, winter conditions with constant indoor heating allow campaign lengths around 72 h. For a strong indoor-outdoor temperature difference (e.g. 10 °C) steady-state models provide reliable estimates, and lumped capacitance models are found to suit lower temperature differences or less stable conditions. However, for estimating thermal capacity, fluctuating indoor and outdoor temperatures are preferred and only the distributed capacitance model provides consistent estimates for different time steps and data subsets. The present work might be helpful in establishing future guidelines for the use of dynamic methods with physical interpretation, presenting a case study of a simple well-known wall facing a variety of winter and summer conditions. It might also provide a basis for further research, extending the application of these models to more complex multi-layer walls and/or for the assessment of design scenarios including thermal insulation.

1. Introduction

In the global context of climate emergency, the implementation of energy saving measures in buildings is regarded as a pressing intervention for reducing greenhouse gas emissions [1]. In the last two decades, the European Union has increased thermal insulation requirements and introduced mandatory energy simulations for the certification of new buildings [2]. However, many studies have highlighted a 'performance gap' between simulation outputs and actual energy performance of buildings, drawing particular attention to the thermal performance of building envelopes [3–5]. Recent years have seen a growing interest on the *in situ* characterisation of building envelopes through non-destructive measurements. However, the characterisation of physical properties from monitored data is far from straightforward. The average method as standardised in ISO 9869–1 [6] remains widely used due to its simplicity but requires quasi-steady-state conditions with a large and sustained temperature difference between interior and exterior, which is often unfeasible. As an alternative, a growing number of dynamic analysis methods have been developed in recent years, although their application remains mostly within the academic field. Reviews of current assessment methods for the thermal performance of building walls are provided in [7–9]. Many of these methods require the control of indoor air temperature through devices mounted over the wall [10,11] or a specific sequence of indoor conditions, e.g. heating with constant power followed by a cooling phase [12,13] or a triangular temperature sequence [14].

Data analysis methods can be classified in accordance to the *greyness* of their underlying models [15]. White-box models are based on prior knowledge from building physics, and the experimental data is expected to validate this previously formulated model. On the contrary, black-box

* Corresponding author at: TECNALIA, Basque Research and Technology Alliance (BRTA), Astondo bidea 700, Bizkaia Science and Technology Park, Derio 48160, Spain.
E-mail address: benat.arregi@tecnalia.com (B. Arregi).

https://doi.org/10.1016/j.enbuild.2023.113393
Received 2 January 2023; Received in revised form 24 June 2023; Accepted 23 July 2023
Available online 27 July 2023
0378-7788/

models are purely data-driven, and aim at finding the functional relation between inputs and outputs without consideration for the physical interpretation of the model. The latter comprise response factors [16], conduction transfer functions (CTF) [17] and autoregressive models (ARX [18] or ARMAX [19]), along with more recent machine learning and deep learning algorithms, such as random forests [20] or artificial neural networks (ANN) [21,22]. A major drawback of black-box models is that, given their dependence on training data, they cannot predict dynamic thermal response for hypothetical scenarios in which the wall assembly is physically modified (e.g. addition of internal or external insulation), which is of great interest for energy-focused renovations.

Grey-box or hybrid models, combining physical interpretation with statistical methods, have become very popular in recent years for both whole building [23–26] and building envelope [27–29] assessment. They are commonly articulated as resistance–capacitance (RC) networks, where the thermal capacitance of the envelope assembly is lumped at one or more nodes. Such models are able to describe the thermal response of thermal systems at high time resolution [30], and can be articulated in deterministic [31] or stochastic [27] form. According to Yu et al. [32], deterministic models appear to work better for prediction and control, while stochastic models would be more suitable for the characterisation of thermal systems.

Models with fully physical representation consider that thermal capacitance is distributed along the whole thickness of the wall. Most applications of distributed capacitance models are formulated in the frequency domain, where Fourier or Laplace transforms allow the use of the elegant quadrupole equations in ISO 13786 [33]. However, their application is often limited to sinusoidal temperature variations of a single frequency, typically 24 h [34–36], representing either theoretical or highly controlled laboratory conditions. Extensions to this method have been proposed to overcome this limitation, such as the addition of further discrete sinusoidal frequencies [37] or a phasor approach covering the continuous frequency range [38]. Time domain methods are superior in terms of practical application and physical interpretation, but analytical solutions of the heat equation have not yet found their application in the building field [39,40], so current distributed capacitance methods are based on numerical solutions for equivalent homogeneous walls [41–44].

In most literature works, the use of dynamic methods is aimed at obtaining a quicker and/or more robust estimation of the thermal resistance of the wall. However, model parameters may contain potentially valuable information on the dynamics of the wall, which is often not evaluated or reported. The present research focuses on the use of *in situ* analysis methods for building envelopes to estimate not only steady-state thermal resistance but also thermal capacitance. For this purpose, the application of three physically interpretable models is investigated: (1) a steady-state model based on the standard average method, (2) a lumped capacitance model within a stochastic framework, and (3) a distributed capacitance model with an analytical solution for step response functions in the time domain. Whereas he first two models are sourced from standards and literature, the specific formulation and application of the distributed capacitance model is a novelty of this study. The performance of these models is investigated and compared for a variety of typical seasonal weather and indoor conditions, monitoring campaign durations, and time steps chosen for analysis. This work attempts to cast light on the different characterisation of thermal capacity in lumped and distributed capacitance models and its practical implications.

Heat flux and temperature data are sourced from a full-scale test aimed at the dynamic thermal characterisation of four concrete panels of differing formulation. The experimental set-up is described in Section 2. The analysis methods and their underlying models are described in Section 3. Results and a comparative evaluation are presented in Section 4, in which the influence of the time step chosen for analysis and the duration of the monitoring campaign are also assessed. Finally, a discussion on the findings and the main conclusions of the study are presented in Sections 5 and 6.

2. Experimental set-up

The data in this study is sourced from a blind test performed in the context of the Eco-Binder project [45] assessing the thermal performance of four different formulations of concrete. One of the panels is made from conventional concrete with Ordinary Portland Cement (OPC) as a binder, while the three others are concrete samples from different manufacturers using Belite-Ye'elimite-Ferrite (BYF) binders of lower carbon footprint. With the aim of characterising their dynamic thermal performance when exposed to realistic outdoor and indoor exposure conditions, panels of identical geometry were produced and subsequently installed in the Kubik experimental facility at Tecnalia's headquarters near Bilbao (43°17′ N 2°52′ W) [46,47]. The building is exposed to an oceanic climate (*Cfb* in the Köppen-Geiger classification) representative of Western Europe [48].

The four concrete panels were installed side by side on the east-facing façade of Kubik, partially forming the external envelope of a large non-partitioned space in the second floor of the building (Fig. 1). The remainder of the façade of this room is a large glazed area oriented to the south and east. The panels have dimensions of 638 mm (width) × 3650 mm (height) × 200 mm (thickness). To mitigate the effects of thermal bridges at the edges of each panel, 50 mm wide extruded polystyrene inserts were placed all around the perimeter of each panel, including junctions between panels, and sealed with polyurethane foam insulation. After the placement of the concrete panels and the perimeter insulation, an external render and a reflective paint coating were applied on site with a trowel and roller brush. The raw concrete constitutes the internal finish to the room side and no further insulation was applied over the panels, to facilitate the identification of the thermal properties of the concrete.

Monitoring equipment was placed at two different heights within each panel (Fig. 2). Heat flux (q_{si}) was monitored with transducers (Phymeas Type 7, measuring area 90 × 90 mm, accuracy ± 5%) placed in direct contact with the internal surface of the wall. Temperatures were monitored using RTD sensors (Heraeus M222 in 4-wire connection, accuracy ± 0.1 K) over the internal surface of the concrete panel (T_{si}) and the external surface of the concrete panel (T_{se}) embedded in a groove behind the external render. External ambient temperature (T_e) was recorded from the weather station of Kubik (Vaisala WXT520, accuracy ± 0.3 K), and indoor ambient temperature (T_i) was monitored using a combination of temperature sensors placed at different heights to measure air stratification (Heraeus M222 in 4-wire connection, accuracy ± 0.1 K). All signals were sampled every second and 60 s averages were recorded onto a programmable logic controller (PLC).

Test conditions at the Kubik test facility are determined by the external weather and the interplay with HVAC systems and use schedules of the building, as opposed to the controlled climate of laboratory tests. The top plot in Fig. 3 presents ambient temperatures monitored over the whole length of the experiment, providing boundary conditions for the test. External temperature readings show marked day-night cycles as well as a clear seasonal variation from winter to summer. Internal air temperatures were controlled by means of fan coil units installed at ceiling level, delivering warm or cool air as required. A variety of indoor conditions were set over the duration of the experiment:

- Phase 1, with free-floating temperature in winter (no heating).
- Phase 2, a heating period with a set point temperature of 21 ± 1 °C, replicating typical indoor comfort conditions.
- Phase 3, a heating period with a set point temperature of 25 ± 1 °C at the top end of the comfort range, aimed at exacerbating heat flow across the experimented wall.
- Phase 4, a sequence switching to free-floating, then cooling (set point 17 ± 1 °C), heating (set point 25 ± 1 °C) and back to cooling (set

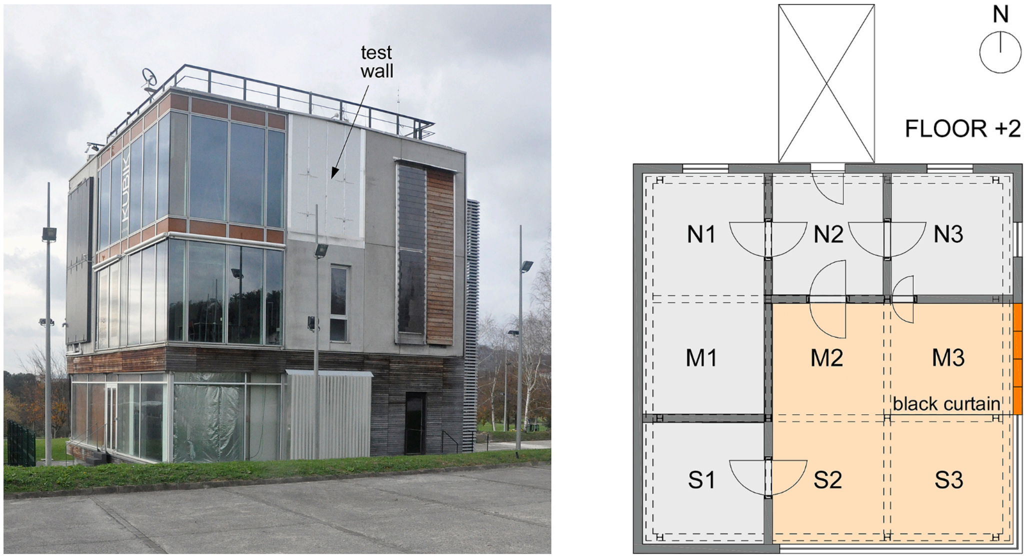

Fig. 1. External view (left) and plan (right) of placement of concrete panels in the building.

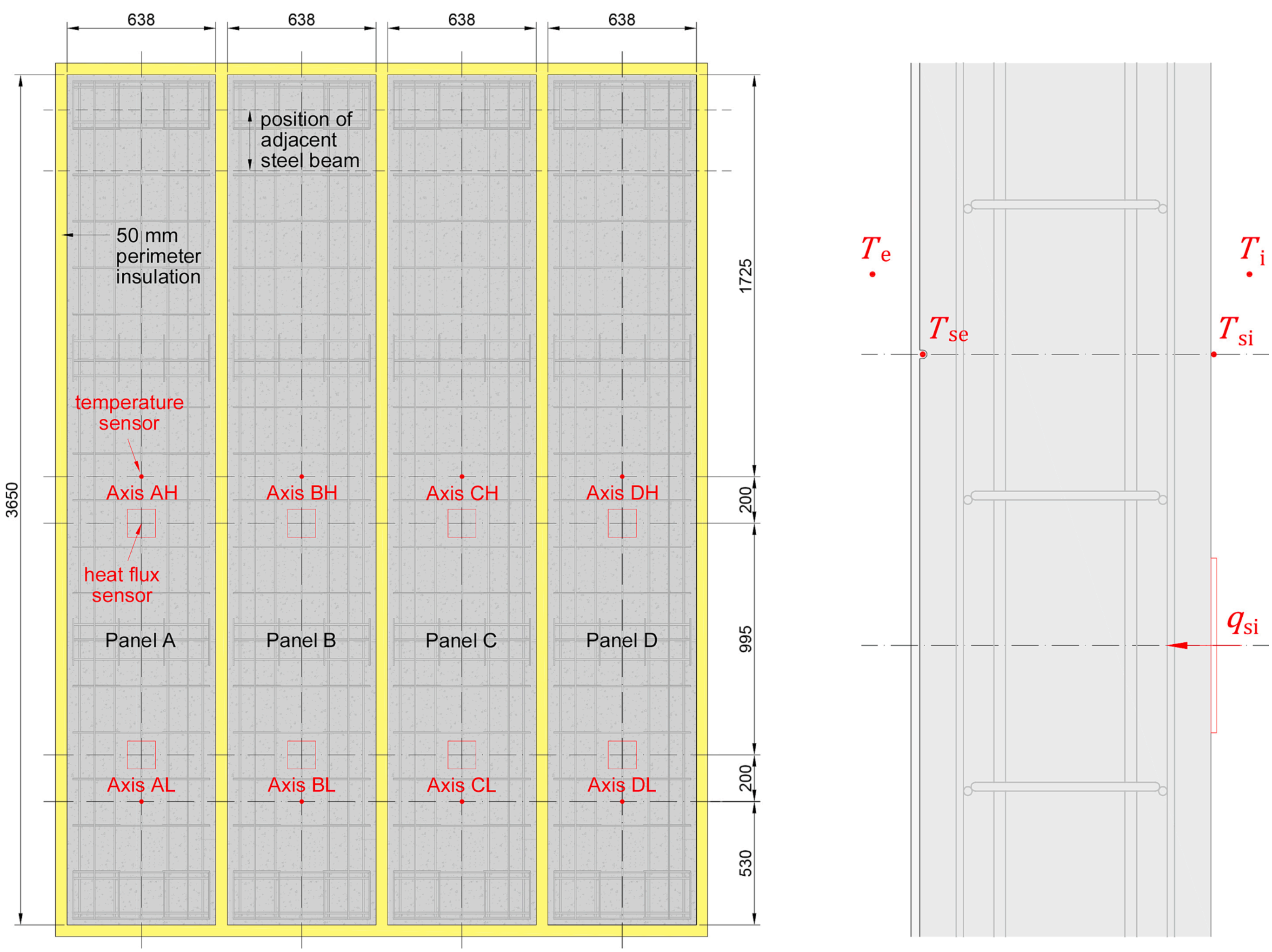

Fig. 2. Location of monitoring devices within internal elevation (left) and vertical section (right).

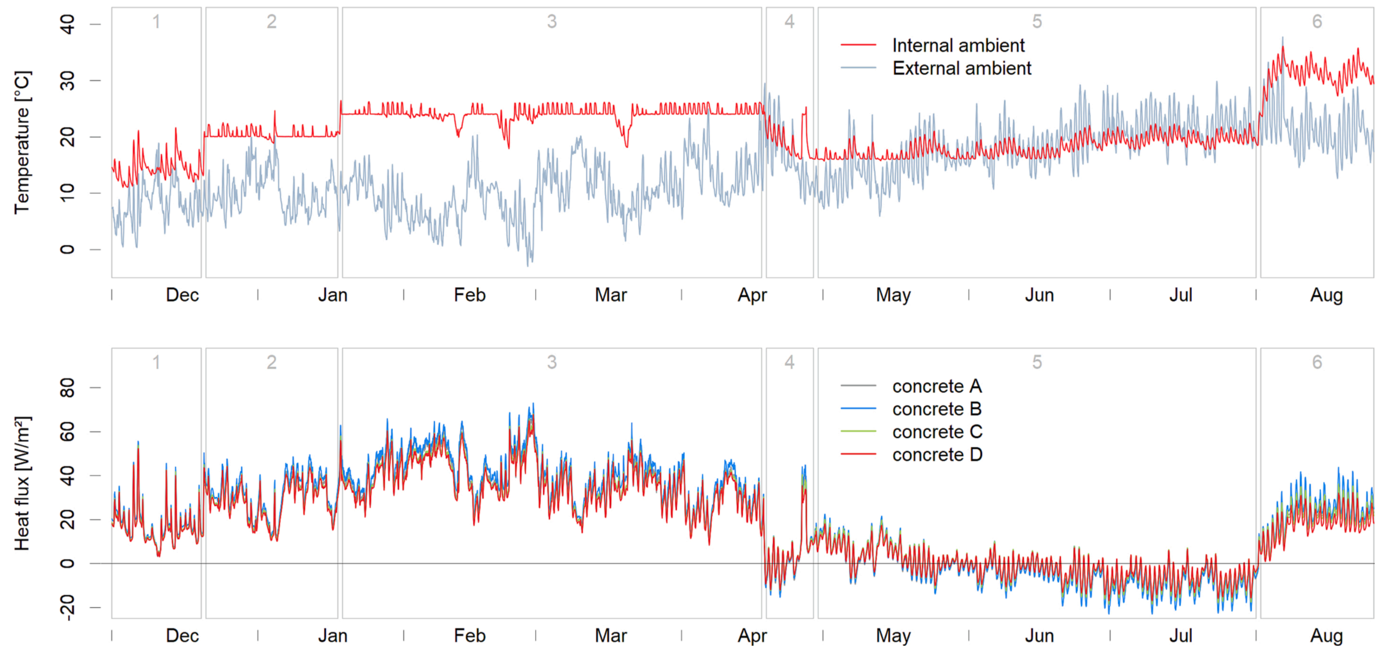

Fig. 3. Boundary temperatures (top) and heat flux (bottom) monitored at the experiment.

point 17 ± 1 °C), aimed at capturing the transient thermal performance of the wall.
- Phase 5, a cooling period aimed at capturing the summer performance of the wall with a set point temperature of 17 ± 1 °C (albeit it is seldom achieved due to the limited cooling power and the high solar aperture of the room).
- Phase 6, with free-floating temperature in summer (no cooling), where the internal air is primarily heated by solar radiation through the large glazed surfaces of the room.

Table 1 indicates the duration and ambient conditions for the whole length of the experiment and within each of the indoor temperature settings described above.

Heat flux measurements tracked during the whole length of the experiment are plotted in the bottom graph of Fig. 3. A positive sign indicates outwards heat flow (consistent for Phases 1, 2, 3 and 6), while a negative sign indicates inwards heat flow. During Phases 4 and 5 heat flow frequently changes direction, which is consistent with expectations from ambient temperatures in the above plot. Overlaid to these clear seasonal trends, significant day/night variations in heat flow can be observed. Heat fluxes follow a similar shape for all four concrete formulations, albeit magnitudes differ slightly (concrete B presenting highest heat flows and concrete D lowest).

The scatter plots in Fig. 4 reveal a strong correlation between indoor-outdoor temperature difference (horizontal axis) and heat flux (vertical axis), which is especially pronounced when daily averages are considered (solid dots). Hourly averages (hollow dots) are affected by dynamic storage effects, showing that instant values of heat flux and temperature difference are decoupled due to the heat absorbed or released by the concrete. All four formulations of concrete show a very similar behaviour. The slope of the correlation is indicative of the thermal transmittance (more conductive for concrete B), while the dispersion of the points around the correlation line is associated with thermal capacitance. Fig. 4 graphically demonstrates that most inertial effects are short-termed and have low impact over the daily cycle (solid dots).

3. Models and methods

The thermal properties of the concrete panel are inferred from temperature measurements at both surfaces (T_{si}, T_{se}) and heat flux measured at the internal surface (q_{si}), which is exposed to the room (Fig. 2). The assessment is limited to the concrete panel, excluding potential sources of distortion from convective and radiative effects. The underlying physical models considered in this study and their corresponding parameter estimation methods are described below.

3.1. Steady-state model

The steady-state model assumes constant boundary temperatures at internal and external surfaces (T_{si}, T_{se}), with a resulting heat flux q that is constant and uniform along the thickness of the wall. A linear relationship between temperature gradient and heat flux is characterised by the thermal resistance R as per Eq. (1). However, stable boundary temperatures are not representative of typical service conditions of

Table 1
Conditions along whole experimental campaign (top row) and phases of varying indoor temperature settings.

	Start date	End date	Length (days)	Ext. daily temperature (°C)			Int. daily temperature (°C)		
				min.	mean	max.	min.	mean	max.
Total	2017–12-01	2018–08-25	268	0.0	14.2	26.7	11.7	21.4	33.7
Phase 1	2017–12-01	2017–12-19	18	3.8	8.1	14.6	11.7	14.3	17.1
Phase 2	2017–12-21	2018–01-17	27	6.1	10.3	16.3	19.7	20.4	21.0
Phase 3	2018–01-19	2018–04-17	88	0.0	10.1	19.7	19.5	24.1	25.2
Phase 4	2018–04-19	2018–04-27	9	11.7	17.0	22.9	16.7	19.5	21.5
Phase 5	2018–04-29	2018–07-31	92	9.1	18.4	23.8	16.1	18.2	20.7
Phase 6	2018–08-02	2018–08-25	23	18.1	21.6	26.7	26.3	31.3	33.7

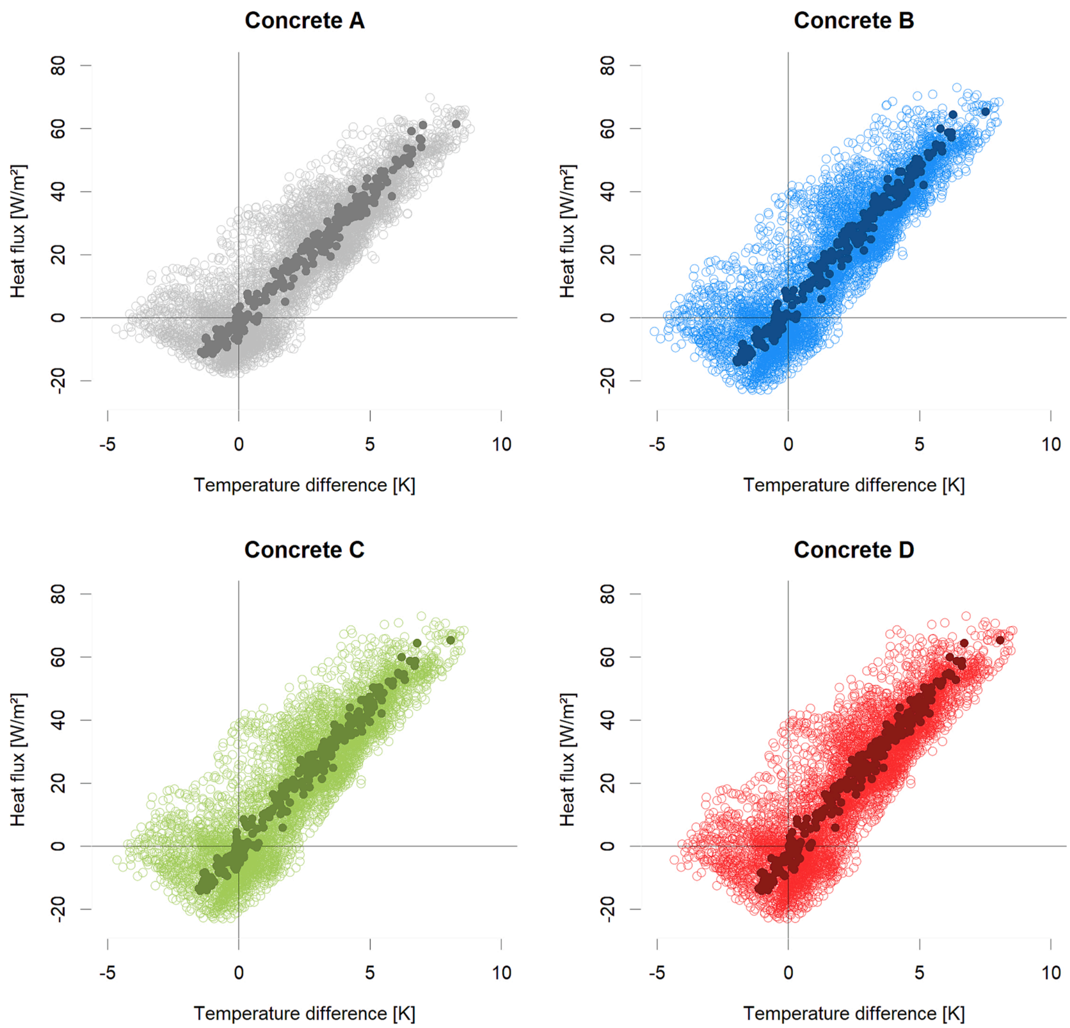

Fig. 4. Heat flux as a function of indoor-outdoor temperature difference: hourly averages (hollow dots), daily averages (solid dots).

envelope assemblies, which face a continuously changing external weather. The average method, standardised in ISO 9869–1 [6], aims at filtering out the dynamics of the system by measuring a sufficiently large number K of time steps k. The standard also provides a set of criteria to estimate whether the campaign length is sufficient to obtain a reasonable estimate of R using Eq. (2).

$$q = \frac{T_{si} - T_{se}}{R} \tag{1}$$

$$R \approx \frac{\sum_{k=0}^{K}\left(T_{si,k} - T_{se,k}\right)}{\sum_{k=0}^{K} q_{si,k}} \tag{2}$$

The average method is widely used because it is simple and easy to implement, but it is affected by many drawbacks. Firstly, in order to get robust results and limit the influence of systematic errors [49], a large and stable temperature difference needs to be maintained, avoiding dynamic effects such as temperature peaks induced by solar radiation. Hence, in practice, winter conditions are advisable and heating to a constant set point temperature is often necessary [8]. The required campaign length depends on the boundary conditions, as well as the thermal characteristics of the assembly, and tends to be longer than for other methods [50]. Moreover, as the model is aimed at filtering out the dynamics, no indication of thermal capacity is provided [51].

3.2. Lumped capacitance model

Lumped capacitance models dissociate thermal resistance and capacity, so that the thermal system can be described by a set of ordinary differential equations (ODE). An electrical analogy is often used, representing the thermal model as a Cauer circuit with electric resistors and capacitors [52]. For building walls, the physical system is often represented using a state-space model where measured boundary temperatures are the input variables, heat flux is the output variable, and the state variables are unmeasured intermediate temperatures at the lumped capacitances. The parameters of the model are a series of thermal resistances R and lumped thermal capacitances C. Assuming one-dimensional heat transfer, the heat balance at each lumped capacitance node n has the form of an ODE in continuous time as shown in Eq. (3). The full set of equations can be written into a matrix formulation, and once solved, the heat flux at the internal surface for each discrete time step k can be estimated from the temperature of the node closest to the internal surface as per Eq. (4).

$$C_n \frac{dT_n}{dt} = \frac{T_{n-1} - T_n}{R_{n-1,n}} + \frac{T_{n+1} - T_n}{R_{n,n+1}} \tag{3}$$

$$q_{si,k} = \frac{1}{R_{si,1}}\left(T_{si,k} - T_{1,k}\right) \tag{4}$$

In this study, estimations of thermal parameters are obtained using a stochastic state-space model with a single lumped capacitance. The system equation for each node is formulated as a linear stochastic differential equation (SDE) in continuous time (Eq. (5)), where the state T_C relates to the temperature at the lumped thermal capacitance, and w_C is an additive noise term (a Wiener process increasing its variance with time [53]). The observation equation (Eq. (6)) is formulated in discrete time, with a measurement error e assumed as a white noise process.

$$dT_C(t) = \left[\frac{T_{si}(t) - T_C(t)}{CR\phi} + \frac{T_{se}(t) - T_C(t)}{CR(1-\phi)}\right]dt + dw_C(t) \quad (5)$$

$$q_{si,k} = \frac{T_{si,k} - T_{C,k}}{R\phi} + e_k \quad (6)$$

A model with a single lumped capacitance has been adopted in this study for the sake of simplicity, aimed at limiting the total number of parameters required to describe the system. Models of two or more lumped capacitances can be implemented by formulating a set of system equations, one per each lumped capacitance, as per Eq. (3).

This model describes the dynamic thermal performance of the wall using three parameters: the thermal resistance R, a lumped thermal capacitance C, and a parameter ϕ (termed accessibility in [54]) describing the location of the lumped capacitance within the thermal resistance of the wall. These parameters have been estimated through the maximum likelihood method through an extended Kalman filter, using the CTSM-R toolkit [55].

3.3. Distributed capacitance model

Lastly, a distributed capacitance model is formulated assuming the concrete as a thermally homogeneous layer with thermal resistance and capacity uniformly distributed along its thickness. While this is not strictly true (most construction products contain non-homogeneities, in this case reinforcement bars), the model provides a reasonable balance between complexity and representativeness.

The heat equation is a partial differential equation (PDE) in the time domain [39]. For a homogeneous layer of distributed capacitance, an analytical solution can be formulated based on infinite decay times expressed as a convergent summation. The analytical solution described in Eq. (7) and Eq. (8) has been derived and adapted from previous works [30,39,56,57]. Let us assume that the wall is at a uniform and stable temperature, and $u(t)$ is a step excitation at $t = 0$ causing an instant temperature increase of ΔT at one boundary, while the opposite boundary remains at the same temperature. We can then define analytical step response functions describing transient heat flux at the internal surface as a response to such step excitations either at the internal (Eq. (7)) or at the external surface (Eq. (8)). The equations contain a steady-state term related to thermal resistance R, and a transient term consisting of a sum of decaying components.

$$h_{s,ii}(t) = \frac{q_{si}(t)}{\Delta T_{si}} = \frac{1}{R} + \frac{2}{R}\sum_{j=1}^{\infty} exp\left[-(j\pi)^2\frac{t}{CR}\right] \quad (7)$$

$$h_{s,ie}(t) = \frac{q_{si}(t)}{\Delta T_{se}} = \frac{1}{R} - \frac{2}{R}\sum_{j=1}^{\infty}(-1)^{j-1} exp\left[-(j\pi)^2\frac{t}{CR}\right] \quad (8)$$

The analytical step response functions of Eq. (7) and Eq. (8) are graphically shown in Fig. 5. While the long-term response is solely dependent on thermal resistance R, the length of the transient period depends on the product of thermal capacity C and resistance R. In the experiment, boundary temperatures ($T_{si,k}$ and $T_{se,k}$) and heat fluxes ($q_{si,k}$) are recorded as a series of discrete values. Provided that these represent average values at each time bin k (spanning one hour in this study), the input can be regarded as a series of instant temperature steps at each time step k. The impact of each step on heat flux can be calculated from bin averages of the step response function (Fig. 5 right), thus eluding the problem of an infinite value at $t = 0$. Since the system is linear, the response $q_{si,k}$ of the wall to any arbitrary time-varying boundary conditions $T_{si,k}$ and $T_{se,k}$ can be obtained as a convolution sum of previous temperature increments.

Within the distributed capacitance model, the dynamic thermal performance of the wall is described using only two parameters with direct physical significance: the thermal resistance R and the distributed thermal capacity C. Given the simplicity of the model, these can be obtained through a straightforward optimisation routine minimising deviation between prediction and measurement.

3.4. Assessment of model quality

The following criteria introduced in [58] have been adopted for model validation:

1. **Simplicity:** Smaller models are preferable, limiting the number of parameters insofar as reasonable.
2. **Identifiability:** Models should allow the determination of their parameters uniquely from the data.
3. **Fit to the data:** Models should be able to explain most of the variance in the data.
4. **Internal validity:** The model should remain reliable when exposed to new conditions (test data) different than those used for parameter estimation (training data).
5. **External validity:** Results obtained with the models should not conflict with previous knowledge or experience without a well justified explanation.
6. **Dynamic stability:** For dynamic models, transients effect induced by temporary variations in input variables should fade out over time.

The models proposed in this study pursue simplicity by character-

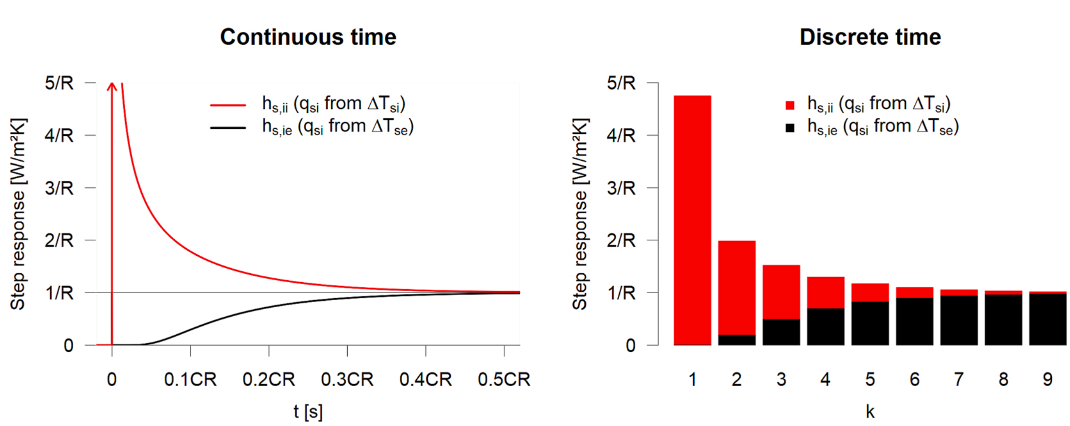

Fig. 5. Step response functions for distributed thermal capacitance in continuous time (left) and discrete time (right).

ising thermal performance through a very restrained set of parameters (1 to 3). The steady-state model has thermal resistance (R) as its only parameter. The distributed capacitance model adds a uniformly distributed thermal capacitance (C) describing dynamic thermal performance. Finally, the lumped capacitance model has 3 parameters: thermal resistance (R) and a thermal capacitance (C) lumped at a fixed position (ϕ) within the wall thickness.

Identifiability of the thermal performance of building walls is closely linked to the boundary conditions, particularly temperature difference [8]. Each assessment method has been applied over the whole monitored period (December 2017 to August 2018) as well as over each of the constituting months. The latter have been selected as subsets of the data with similar duration but varying exposure conditions. Model identifiability is assessed by checking whether parameters can be obtained for all or most months, are consistent among different months, and meet the convergence criteria of the relevant estimation method. The assumption of constant thermal properties for each concrete sample is necessary for preserving the linearity of the models and has been considered a reasonable simplification. In reality, there is some affection by temperature and moisture content, which might result in variations of thermal resistance and capacitance over different seasons and even over different depths within the wall.

For assessing the fit of the model estimates within the measured data, two complementary metrics have been used: the coefficient of determination R^2 and the coefficient of variation of the root mean square deviation CV(RMSD). These indicators are well known [59] and have been applied in other research works in the field [60,61]. The former measures the fraction of the variance that is explained by the model (with a value of 1 indicating a perfect fit to the data). The latter is a measure of the average deviation between model estimates and predictions, with lower values (close to zero) indicating a more accurate model.

Regarding internal validity, the consistency of the parameter estimations is initially assessed by tracking their variability among monthly estimations. This allows for testing the sensitivity of the parameter estimates to seasonal weather patterns and indoor conditions. For a further assessment of the prediction capability of each model when exposed to new conditions, the coefficient of variation of the root mean squared error CV(RMSE) is adopted as a metric. This is equivalent to the CV (RMSD), except predictions are made over a different dataset than the one used for fitting the model, again under the assumption of time-invariant thermal properties.

The external validity of the models is assessed through a plausibility check of the results, contrasting the obtained parameters (thermal resistance and capacitance) with values in literature. This is feasible since the parameters of the selected models have direct physical interpretation. Thermal conductivity estimates (in units of W/m·K) are obtained dividing panel thickness by thermal resistance. Volumetric heat capacities (in units of J/m^3·K) are obtained dividing lumped and distributed thermal capacitances (which are areal values) by panel thickness. Further parameters of interest, such as thermal diffusivity and effusivity, can also be readily obtained from these values.

The choice of models built on algebraic or differential equations allows a direct evaluation of dynamic stability. This is performed by formulating the continuous-time response of the system (heat flux through the internal surface) to a step increase in temperature at each side, and checking that values converge over time towards the steady-state assumption.

4. Results and analysis

4.1. Parameter estimation and identifiability

Thermal resistance estimates obtained with the steady-state model are listed in Table 2. Omitted values did not met the convergence criteria stated in the standard [6]. When considering the whole set of data, only one of the four concrete formulations meets the validity criteria. Monthly and annual estimates are presented in the top left plot of Fig. 6, including those that did not meet the convergence criteria (white bars with lighter contour). Monthly estimates obtained in winter (with high temperature differences between the boundaries) are reasonably consistent, especially for concretes A and D, but summer estimates diverge considerably for most cases (even those that comply with convergence criteria, e.g. July for concrete B or August for concrete D). Possible reasons for this divergence are discussed in Section 5.

Table 2
Total and monthly thermal resistance estimates obtained with the steady-state model.

	Phases	Concrete A	Concrete B	Concrete C	Concrete D
Total	1–6	–	–	$R = 0.1265$ m^{2}K/W	–
Dec	1, 2	$R = 0.1269$ m^{2}K/W	$R = 0.0909$ m^{2}K/W	$R = 0.1233$ m^{2}K/W	$R = 0.1361$ m^{2}K/W
Jan	2, 3	$R = 0.1260$ m^{2}K/W	$R = 0.0992$ m^{2}K/W	$R = 0.1280$ m^{2}K/W	$R = 0.1374$ m^{2}K/W
Feb	3	$R = 0.1262$ m^{2}K/W	$R = 0.1050$ m^{2}K/W	$R = 0.1301$ m^{2}K/W	$R = 0.1388$ m^{2}K/W
Mar	3	$R = 0.1266$ m^{2}K/W	$R = 0.1006$ m^{2}K/W	$R = 0.1271$ m^{2}K/W	$R = 0.1375$ m^{2}K/W
Apr	3–5	–	$R = 0.0952$ m^{2}K/W	$R = 0.1285$ m^{2}K/W	–
May	5	–	–	$R = 0.1157$ m^{2}K/W	–
Jun	5	–	–	–	–
Jul	5	–	$R = 0.1438$ m^{2}K/W	$R = 0.1411$ m^{2}K/W	–
Aug	6	$R = 0.1296$ m^{2}K/W	–	$R = 0.1297$ m^{2}K/W	$R = 0.1595$ m^{2}K/W

The lumped capacitance model provides estimates of thermal resistance R along with two additional parameters: the lumped thermal capacitance C and its relative location within the wall ϕ. The data is shown in Table 3 and presented in the plots of the middle column from Fig. 6. Thermal resistance values are relatively consistent, particularly in winter conditions, when a high temperature difference is maintained. However, a high variation among months is observed for the lumped thermal capacitance C and its relative position ϕ. Moreover, both parameters appear to be correlated, as higher estimates of C are obtained when the estimated position ϕ is closer to the external face of the wall (e.g. May for concretes A and D, June for concrete B).

Lastly, Table 4 and the plots in the right column of Fig. 6 present estimates obtained with the distributed capacitance model. The estimates obtained through the optimisation are those leading to the lowest divergence between model estimates and measured values. Valid estimates of R could not be obtained for the months without a clear temperature difference (May to July). The estimates obtained for the remainder of the months are very close to the values obtained with the lumped capacitance model. For thermal capacitance, estimates obtained with the distributed capacitance model are much more consistent among the different months than for the lumped capacitance model. Indeed, estimates of C obtained with the lumped capacitance model should be regarded as *effective* heat capacitances rather than *true* heat capacitances: this is further discussed in Section 5.

4.2. Fit to the data

The goodness of fit of the three models is evaluated by assessing their coefficient of determination R^2 and the coefficient of variation of the root mean square deviation CV(RMSD), as described in Section 3.4. Monthly values obtained with hourly resolution for all four concrete panels are presented in the plots of Fig. 7. Generally, the four concrete formulations appear to follow an analogous pattern, and the response of each model is very dependent on the exposure conditions. The steady-state model, as expected, shows poor prediction capabilities for

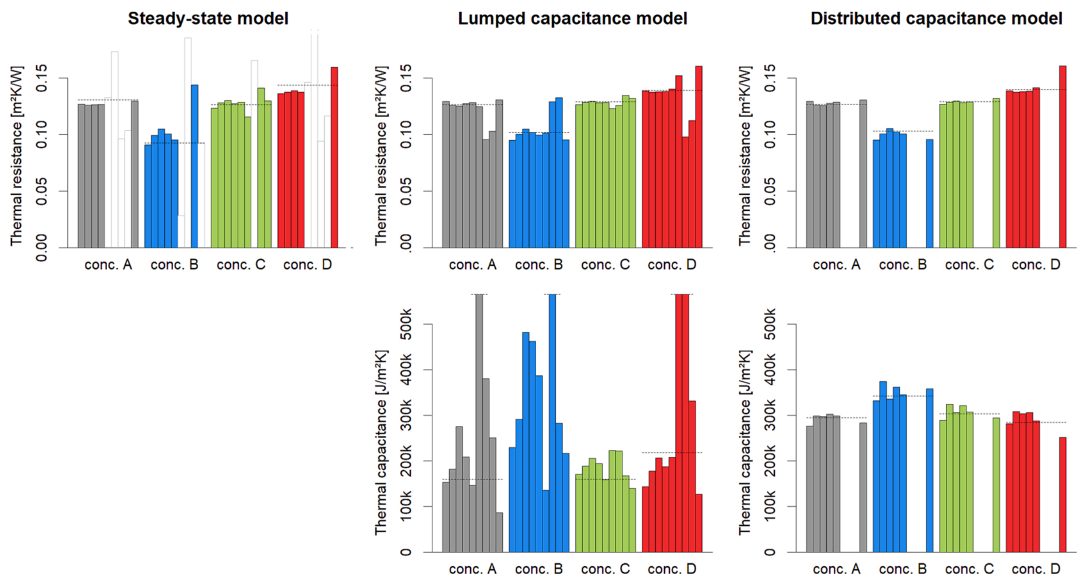

Fig. 6. Thermal resistance (top) and capacitance (bottom) estimates obtained with the steady-state model (left), the lumped capacitance model (centre) and the distributed capacitance model (right) for each month: dotted lines indicate overall period, vertical bars indicate monthly estimates (hollow bars and missing months did not meet convergence criteria).

obtaining hourly estimates. Even for the best results, obtained for months with cold external temperatures, most of the variance remains unexplained according to R^2 values. In these conditions, both dynamic models (lumped and distributed capacitance) achieve a much better fit with R^2 close to 1. However, in the months with lowest temperature difference (June and July) all models fail in achieving a valid CV (RMSD), indicating poor accuracy in such conditions.

4.3. Internal validity

The reliability of a model is not guaranteed by a good prediction capability over the sampling period (training data), but is best assessed by testing the model when facing new conditions outside the sample (test data). For this purpose, a cross validation has been performed by selecting three subsets of the dataset with varying exposure conditions: February 2018 (controlled indoor temperature and greatest heat flow), April 2018 (lower temperature gradient and heat flow reversals), and August 2018 (free-floating temperature with solar heating). Results obtained for the three investigated models (obtained with a one-hour time step) are presented in Table 5.

For the steady-state model, high values of CV(RMSD) and CV(RMSE) can be attributed to the non-inclusion of dynamic effects, and there is no significant difference for predictions within and outside the sample. The lumped capacitance model tends to predict worse outside the sample, especially if the new data presents different exposure conditions. Poorest cross validation results are obtained when the model is trained in winter/spring conditions (February or April) and tested in summer conditions (August), or vice versa. Cross validation is better between February and April, which share a period of artificial indoor heating. In contrast, the distributed capacitance model appears to extrapolate successfully into exposure conditions different to the training data, possible due to its greater physical significance. The only exception is concrete D, which shows a disparity between February-April and August akin to the results obtained with the lumped capacitance model. Possible causes are discussed in Section 5.

4.4. External validity

A plausibility check is performed on thermal conductivity and volumetric heat capacity estimates obtained with each model, by (1) tracking variability of estimates among different months, and (2) comparing such estimates with values in literature. The calculation procedure for obtaining the estimates is described in Section 3.4. The steady-state model is not included since it does not provide heat capacity estimates. In Fig. 8, estimates obtained using the lumped and distributed capacitance models for thermal conductivity (horizontal axis) and volumetric heat capacity (vertical axis) are graphically presented, together with ranges obtained from literature. Regarding the latter, different concrete formulations can result in a broad range of thermal conductivity and heat capacity values [62,63] (region AC in Fig. 8). Despite the relatively wide availability of studies on the thermal conductivity of concrete and cement-based materials, only a limited number among these provide heat capacity measurements [64]. Measurements for a set of mediumweight concretes performed by Cavalline et al., [65] show a much more constrained variance (region MWC in Fig. 8).

Heat capacity estimates obtained with the distributed capacitance model appear much more consistent among them than those obtained with the lumped capacitance model. The only exception is the August measurement for concrete D (on the left of the scatter plot), which is later discussed in Section 5. Furthermore, thermal conductivity and heat capacity estimates obtained with the distributed capacitance model agree well with values from material testing studies.

4.5. Dynamic stability

Fig. 9 presents the dynamic response in continuous time assumed from each of the three models. The plot is built on the parameters fitted for Concrete C, since all three models converged well for the overall data (Tables 2-4). The transient response h_S represents the heat flux through the internal surface (q_{si}) responding to a unit step temperature excitation over the internal (ΔT_{si}) or external (ΔT_{se}) surface.

Dynamic stability is achieved in all cases, with all values converging over time towards the steady-state assumption, which corresponds to the thermal transmittance. When the temperature excitation is on the opposite side, the heat flux response is initially zero and grows gradually towards the equilibrium value. When the temperature excitation is on the same side, the heat flux response experiences an instant peak and then decreases towards the equilibrium value.

Table 3
Total and monthly thermal resistance, lumped capacitance and its relative location estimates obtained with the lumped capacitance model.

	Phases	Concrete A	Concrete B	Concrete C	Concrete D
Total	1–6	$R = 0.1265$ m^{2}K/W $C = 159589$ J/m^{2}K $\phi = 0.3577$	$R = 0.1019$ m^{2}K/W $C = 730527$ J/m^{2}K $\phi = 0.8132$	$R = 0.1288$ m^{2}K/W $C = 160069$ J/m^{2}K $\phi = 0.3371$	$R = 0.1390$ m^{2}K/W $C = 218183$ J/m^{2}K $\phi = 0.4902$
Dec	1–2	$R = 0.1292$ m^{2}K/W $C = 153079$ J/m^{2}K $\phi = 0.3656$	$R = 0.0949$ m^{2}K/W $C = 229637$ J/m^{2}K $\phi = 0.4582$	$R = 0.1265$ m^{2}K/W $C = 170727$ J/m^{2}K $\phi = 0.3805$	$R = 0.1386$ m^{2}K/W $C = 143534$ J/m^{2}K $\phi = 0.3249$
Jan	2–3	$R = 0.1259$ m^{2}K/W $C = 181795$ J/m^{2}K $\phi = 0.4169$	$R = 0.1003$ m^{2}K/W $C = 291228$ J/m^{2}K $\phi = 0.5151$	$R = 0.1284$ m^{2}K/W $C = 188449$ J/m^{2}K $\phi = 0.3659$	$R = 0.1374$ m^{2}K/W $C = 177683$ J/m^{2}K $\phi = 0.3655$
Feb	3	$R = 0.1252$ m^{2}K/W $C = 275140$ J/m^{2}K $\phi = 0.5806$	$R = 0.1049$ m^{2}K/W $C = 482063$ J/m^{2}K $\phi = 0.7251$	$R = 0.1294$ m^{2}K/W $C = 205448$ J/m^{2}K $\phi = 0.4442$	$R = 0.1378$ m^{2}K/W $C = 206434$ J/m^{2}K $\phi = 0.4409$
Mar	3	$R = 0.1272$ m^{2}K/W $C = 208490$ J/m^{2}K $\phi = 0.4755$	$R = 0.1018$ m^{2}K/W $C = 462349$ J/m^{2}K $\phi = 0.7087$	$R = 0.1280$ m^{2}K/W $C = 194224$ J/m^{2}K $\phi = 0.3905$	$R = 0.1382$ m^{2}K/W $C = 187324$ J/m^{2}K $\phi = 0.3928$
Apr	3–5	$R = 0.1283$ m^{2}K/W $C = 146436$ J/m^{2}K $\phi = 0.3141$	$R = 0.0995$ m^{2}K/W $C = 387010$ J/m^{2}K $\phi = 0.6537$	$R = 0.1283$ m^{2}K/W $C = 159100$ J/m^{2}K $\phi = 0.3277$	$R = 0.1403$ m^{2}K/W $C = 207960$ J/m^{2}K $\phi = 0.4678$
May	5	$R = 0.1247$ m^{2}K/W $C = 1680603$ J/m^{2}K $\phi = 0.9329$	$R = 0.1015$ m^{2}K/W $C = 135738$ J/m^{2}K $\phi = 0.2761$	$R = 0.1230$ m^{2}K/W $C = 222929$ J/m^{2}K $\phi = 0.4698$	$R = 0.1520$ m^{2}K/W $C = 1689656$ J/m^{2}K $\phi = 0.9416$
Jun	5	$R = 0.0956$ m^{2}K/W $C = 380289$ J/m^{2}K $\phi = 0.6149$	$R = 0.1290$ m^{2}K/W $C = 1691125$ J/m^{2}K $\phi = 0.9379$	$R = 0.1256$ m^{2}K/W $C = 222002$ J/m^{2}K $\phi = 0.4708$	$R = 0.0979$ m^{2}K/W $C = 1700924$ J/m^{2}K $\phi = 0.9115$
Jul	5	$R = 0.1029$ m^{2}K/W $C = 250908$ J/m^{2}K $\phi = 0.4690$	$R = 0.1326$ m^{2}K/W $C = 282839$ J/m^{2}K $\phi = 0.6255$	$R = 0.1346$ m^{2}K/W $C = 167605$ J/m^{2}K $\phi = 0.3646$	$R = 0.1124$ m^{2}K/W $C = 331497$ J/m^{2}K $\phi = 0.6030$
Aug	6	$R = 0.1306$ m^{2}K/W $C = 86631$ J/m^{2}K $\phi = 0.2282$	$R = 0.0953$ m^{2}K/W $C = 216776$ J/m^{2}K $\phi = 0.4053$	$R = 0.1318$ m^{2}K/W $C = 139756$ J/m^{2}K $\phi = 0.3011$	$R = 0.1605$ m^{2}K/W $C = 127097$ J/m^{2}K $\phi = 0.3134$

4.6. Impact of discrete time step

For characterising the thermal performance of thermal envelope components, temperature and heat flux measurements are usually recorded at fixed intervals. Typically, a fine time resolution (e.g. in the range of seconds) is adopted for monitoring sample measurements, and a smaller resolution (e.g. in the range of minutes) is used for storing mean measurements within each time bin. Later, the collected data is further resampled for analysis, averaging monitored values at even coarser resolution (e.g. in the range of hours). Heat transfer phenomena in building walls are usually slow-responding [39], and a balance must be sought between reliability and computational requirements. In this study, an hourly time step has been initially adopted for analysis for the dynamic methods using lumped and distributed capacitance models (estimates from steady-state models are unaffected by the choice of time step, since they work from an average of the whole dataset). In this section, a further analysis is performed by fitting these same models

Table 4
Total and monthly thermal resistance and distributed capacitance estimates obtained with the distributed capacitance model.

	Phases	Concrete A	Concrete B	Concrete C	Concrete D
Total	1–6	$R = 0.1268$ m^{2}K/W $C = 294768$ J/m^{2}K	$R = 0.1030$ m^{2}K/W $C = 342227$ J/m^{2}K	$R = 0.1291$ m^{2}K/W $C = 303268$ J/m^{2}K	$R = 0.1396$ m^{2}K/W $C = 284316$ J/m^{2}K
Dec	1, 2	$R = 0.1293$ m^{2}K/W $C = 276371$ J/m^{2}K	$R = 0.0952$ m^{2}K/W $C = 332126$ J/m^{2}K	$R = 0.1268$ m^{2}K/W $C = 289003$ J/m^{2}K	$R = 0.1387$ m^{2}K/W $C = 281856$ J/m^{2}K
Jan	2, 3	$R = 0.1261$ m^{2}K/W $C = 298359$ J/m^{2}K	$R = 0.1006$ m^{2}K/W $C = 374501$ J/m^{2}K	$R = 0.1286$ m^{2}K/W $C = 324347$ J/m^{2}K	$R = 0.1375$ m^{2}K/W $C = 308251$ J/m^{2}K
Feb	3	$R = 0.1256$ m^{2}K/W $C = 297155$ J/m^{2}K	$R = 0.1052$ m^{2}K/W $C = 335847$ J/m^{2}K	$R = 0.1296$ m^{2}K/W $C = 306147$ J/m^{2}K	$R = 0.1379$ m^{2}K/W $C = 303467$ J/m^{2}K
Mar	3	$R = 0.1275$ m^{2}K/W $C = 302464$ J/m^{2}K	$R = 0.1023$ m^{2}K/W $C = 361963$ J/m^{2}K	$R = 0.1283$ m^{2}K/W $C = 321428$ J/m^{2}K	$R = 0.1383$ m^{2}K/W $C = 306182$ J/m^{2}K
Apr	3–5	$R = 0.1286$ m^{2}K/W $C = 298461$ J/m^{2}K	$R = 0.1005$ m^{2}K/W $C = 345064$ J/m^{2}K	$R = 0.1287$ m^{2}K/W $C = 307194$ J/m^{2}K	$R = 0.1413$ m^{2}K/W $C = 287795$ J/m^{2}K
May	5	–	–	–	–
Jun	5	–	–	–	–
Jul	5	–	–	–	–
Aug	6	$R = 0.1305$ m^{2}K/W $C = 283225$ J/m^{2}K	$R = 0.0956$ m^{2}K/W $C = 358432$ J/m^{2}K	$R = 0.1319$ m^{2}K/W $C = 294418$ J/m^{2}K	$R = 0.1606$ m^{2}K/W $C = 251517$ J/m^{2}K

using a range of different time steps (from 5 min to 24 h) and assessing the effect of this choice on the obtained parameter estimates. The three subsets of the data previously used for cross validation (February, August and April 2018) have been selected for this analysis, since they are representative of different exposure conditions.

Fig. 10 presents parameter estimates obtained for each model and concrete formulation as a function of the chosen time step. Thermal resistance estimates obtained with the three models are very close to each other, excepting a slight deviation of the steady-state model for some concretes (B, D) in April. The choice of the time step does not seem to affect estimates of thermal resistance, except for a slight but anomalous increase in the estimates provided by the distributed capacitance model in August at a time interval of 6 h. However, regarding thermal capacitance, results from the lumped and distributed capacitance models present significant differences (steady-state models discard heat capacity). Estimates obtained with the distributed capacitance method are rather consistent among different time steps, and particularly around time intervals in the range of one hour. In contrast, the lumped capacitance method yields different capacity estimates in function of the time step chosen.

Comparing the values for the estimates obtained for different months, the relative thermal performance of the four concrete samples seems to differ more as time goes on. All models agree on a relatively consistent thermal resistance of concrete A and C among the 3 months assessed. However, thermal resistance of concrete D seems to increase, while that of concrete B decreases. Thermal capacitances obtained with the distributed capacitance method show a corresponding opposite effect: relatively constant capacity for concretes A and C, a decrease for concrete D, and an increase for concrete B. A possible explanation is presented in Section 5.

4.7. Impact of campaign duration

This section assesses the campaign time required for fitting each of

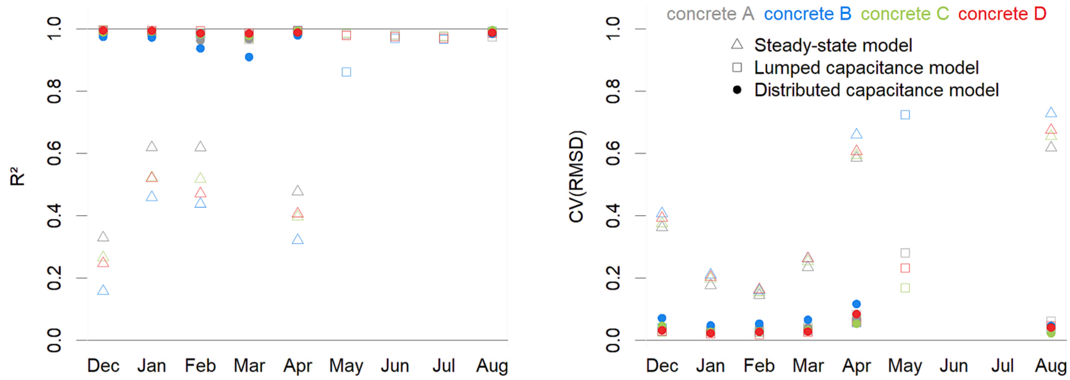

Fig. 7. Assessment of goodness of fit of the studied models with hourly resolution.

Table 5
CV(RMSD) within training data (values in brackets) and CV(RMSE) outside training data (for cross validation).

Training data		Test data			Test data			Test data		
		Steady-state model			Lumped capacitance model			Distr. capacitance model		
		Feb 2018	Apr 2018	Aug 2018	Feb 2018	Apr 2018	Aug 2018	Feb 2018	Apr 2018	Aug 2018
Conc. A	Feb 2018	(0.1447)	0.6060	0.6329	(0.0319)	0.1094	0.1928	(0.0453)	0.0762	0.0613
	Apr 2018	0.1523	(0.5852)	0.6055	0.0496	(0.0823)	0.1678	0.0515	(0.0687)	0.0531
	Aug 2018	0.1456	0.5941	(0.6180)	0.1014	0.1874	(0.0613)	0.0596	0.0751	(0.0440)
Conc. B	Feb 2018	(0.1591)	0.6211	0.6733	(0.0260)	0.0608	0.1256	(0.0532)	0.1294	0.1059
	Apr 2018	0.1970	(0.6597)	0.7108	0.0323	(0.0560)	0.1197	0.0717	(0.1163)	0.0684
	Aug 2018	0.2215	0.6797	(0.7284)	0.0887	0.1489	(0.0340)	0.1150	0.1326	(0.0463)
Conc. C	Feb 2018	(0.1536)	0.5928	0.6558	(0.0260)	0.0785	0.1685	(0.0289)	0.0537	0.0338
	Apr 2018	0.1539	(0.5940)	0.6576	0.0310	(0.0707)	0.1593	0.0296	(0.0531)	0.0378
	Aug 2018	0.1535	0.5924	(0.6552)	0.0665	0.1452	(0.0351)	0.0343	0.0628	(0.0223)
Conc. D	Feb 2018	(0.1629)	0.6286	0.7626	(0.0179)	0.0602	0.1673	(0.0267)	0.0926	0.1878
	Apr 2018	0.1695	(0.6066)	0.7186	0.0197	(0.0589)	0.1563	0.0367	(0.0842)	0.1527
	Aug 2018	0.2039	0.5940	(0.6749)	0.1022	0.1708	(0.0466)	0.1478	0.1753	(0.0410)

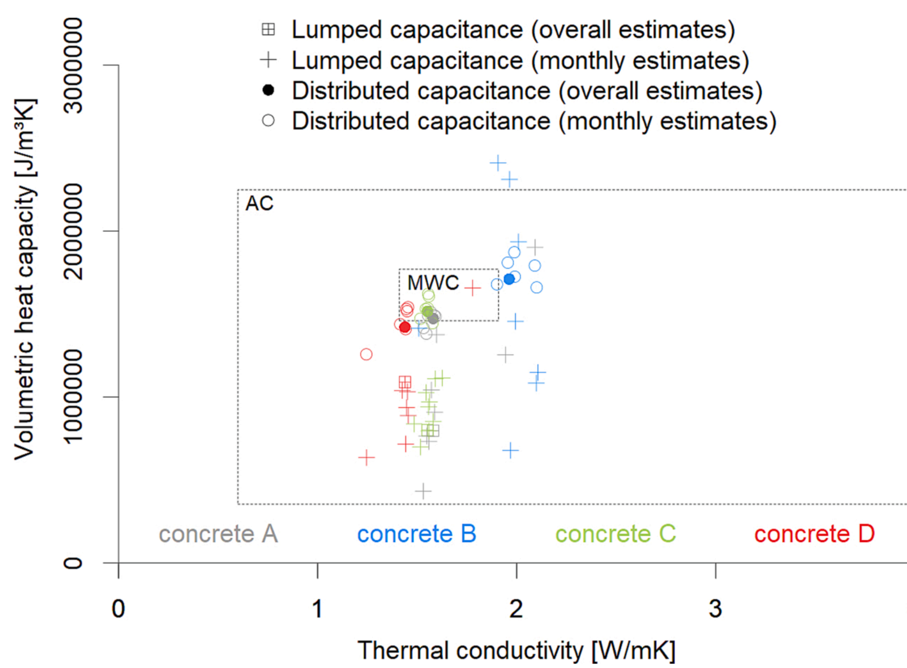

Fig. 8. Scatter plot of thermal conductivity and heat capacity obtained from the lumped and distributed models, compared to values in literature (region AC: all concretes in [62,63], region MWC: middleweight concretes in [65]).

the models and the impact of campaign length on the parameter estimates. In order to find the effect of exposure conditions, the same subsets of the data previously used for cross validation and time step assessment are adopted for this analysis. Results obtained for different campaign durations (from one day up to one month) are presented in Fig. 11. The steady-state and the lumped parameter models can provide

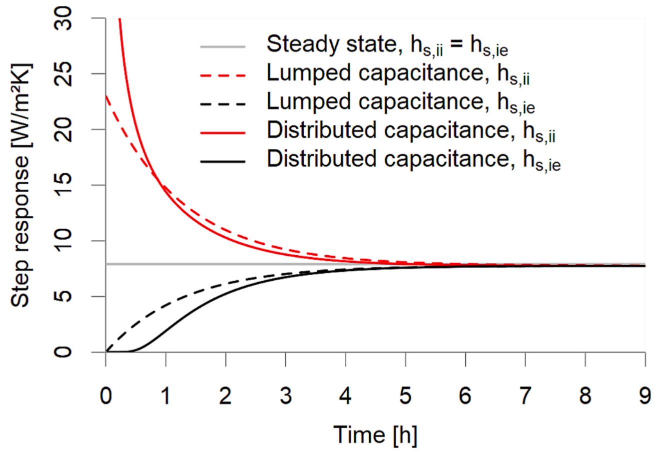

Fig. 9. Step response functions in continuous time, when models are fitted for the data of concrete C within the overall experimental period.

estimates from just 24 h of data, although these are not always reliable. In contrast, the distributed capacitance model requires a longer campaign length (7–10 days depending on exposure conditions) but appears to provide more stable estimates. For February, the dataset with the strongest temperature difference, all three models agree on thermal resistance estimates after 2–3 days of test duration. For April, the average method is less stable and diverges towards the end of the month when conditions become more dynamic (Fig. 3). At the beginning of August, while the wall is heating up (Fig. 3), the average method underestimates thermal resistance. Lumped and distributed capacitance models yield almost identical estimates for thermal resistance. The former can provide a result with a short test duration, but its reliability depends on the stability of test conditions (2–3 days appear to be enough for February and April). The latter requires a longer time to converge but provides very reliable estimates. Thermal capacitance values obtained through the two dynamic methods show an interesting divergence. Estimates from the lumped parameter method fluctuate as the campaign progresses, and values obtained at different months also differ notably. In contrast, the distributed capacitance model, despite requiring longer time to converge, provides much more consistent estimates both within each month and among different data subsets.

5. Discussion

Monitoring conditions with high temperature difference (cold outdoor temperatures and constant indoor heating, e.g. February in Fig. 10) resulted in more robust estimations of thermal resistance and lower requirements for campaign length, in agreement with findings from previous studies [51,66]. The steady-state model performed well in such situations but did not meet the validity criteria of the standard [6] when conditions were more dynamic. Indeed, when considering data from the overall experimental campaign, summer measurements distorted the whole set of data for 3 out of 4 concrete formulations. This confirms that, for the application of the steady-state model, a short campaign with a high temperature gradient is preferable over extending this campaign with an additional period of less suitable conditions. Beyond temperature difference, stability of conditions is also required by the steady-state model: thermal resistance was underestimated when the wall absorbed heat (beginning of August, Fig. 11), and overestimated when the wall released heat (end of April, Fig. 11). This is consistent with observations from a previous study for a much better insulated wall [67]. The single lumped capacitance model applied in this study provided results for all subsets of data, but thermal resistance estimates did not seem reliable for periods when heat flux is low and frequently changes direction, e.g. June and July in Table 3 and top centre chart of Fig. 6. Furthermore, despite the method achieving a good fit, thermal capacitance estimates varied both among different data subsets (bottom row of Fig. 6) and when different time windows and time steps were adopted within a dataset (Fig. 10 and Fig. 11). Lastly, the distributed capacitance model did not converge for the most challenging conditions (low and alternating heat flow, May-July in Table 4), but when estimates were provided, these were consistent for both thermal resistance and capacitance among different data subsets (Fig. 6), time steps (Fig. 10) and campaign lengths (Fig. 11).

Results from lumped and distributed capacitance models diverge mostly in the first instants of the transient process (Fig. 9), and thus discrepancies among these methods would be more significant in exposure conditions with fast frequencies, e.g. rapid changes in

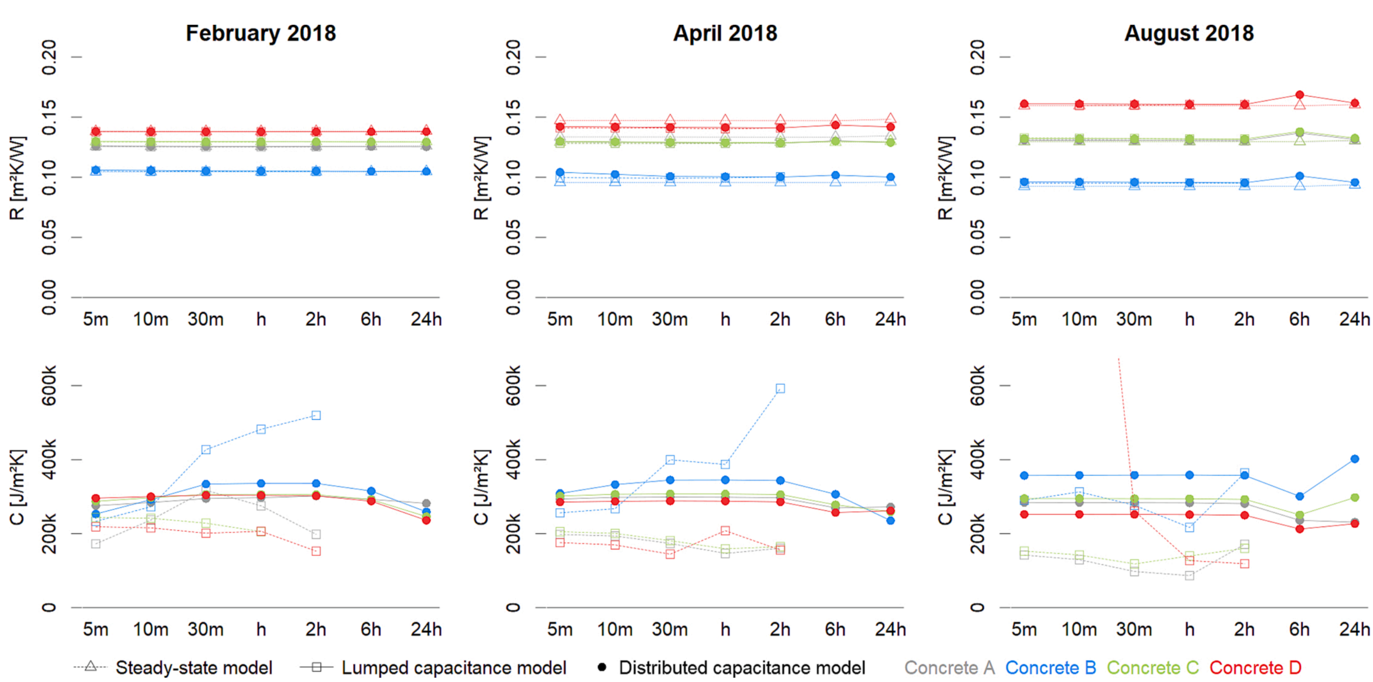

Fig. 10. Thermal resistance (top row) and capacitance (bottom row) estimates obtained with each model for different time intervals.

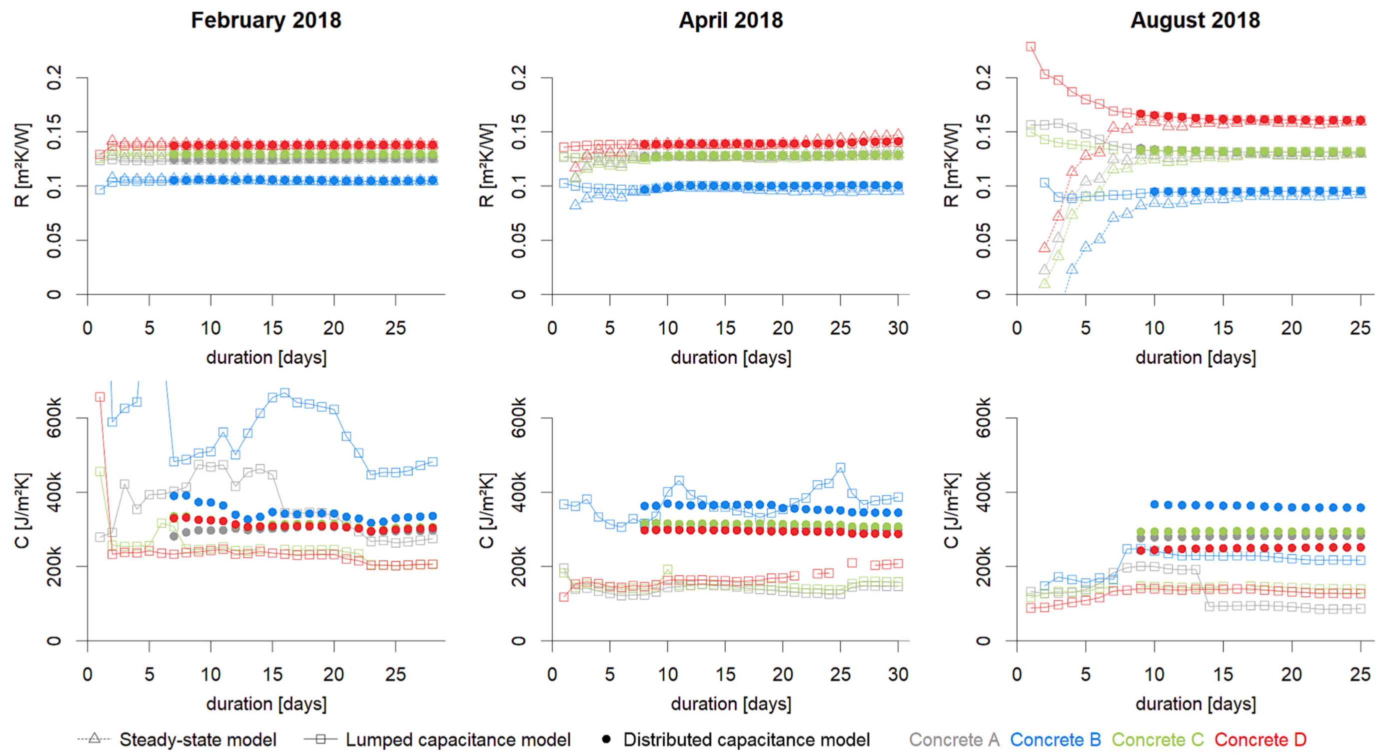

Fig. 11. Thermal resistance (top row) and capacitance (bottom row) estimates obtained with each model for different campaign durations.

temperature. The superior consistency obtained for the distributed capacitance model can be attributed to its underlying physical model, which captures the performance along the whole frequency spectrum. Another distributed capacitance model by Cucumo et al. [41] also yielded consistent results for both thermal resistance and capacitance among different periods. Masy [54] applied a single lumped capacitance model, analogous to the one in this study, in a theoretical study based on a 24 h sinusoidal excitation, and also found the model quick to compute but less reliable at high frequencies. Indeed, a single lumped capacitance model is limited to one exponential decay mode (or *time constant*) as apparent from Fig. 9, which might make the model prone to overfit as the parameters must be 'tuned' to suit the specific exposure conditions. This behaviour can be observed in the results obtained in summer conditions (Table 3), when occasionally the position of the lumped capacitance is 'shifted' towards the external side ($\phi > 0.9$) with capacitance values in the region of 1.7 MJ/m^{2}K (e.g. May and June for Concrete D), which are useful for fitting the data but not physically congruent. Estimations tend to be more reliable if the thermal capacitance is placed closer to the centre of the wall ($\phi \sim 0.5$), but even so, thermal capacitance estimates are lower than those obtained with the distributed capacitance method. Capacity values obtained from the lumped capacitance method are defined by some authors as 'effective heat capacities' [36,68,69]. The findings from the present study appear to indicate that such effective heat capacities are frequency-dependent (vary according to the exposure conditions of the training data), and thus have weaker physical sense than the ones estimated with the distributed capacitance model, which relate to the true physical heat capacity of the wall. A number of experimental [27,70] and theoretical [28,71] studies concluded that models with two lumped capacitances can acceptably reproduce the dynamic response of a wall over the whole range of frequencies encountered in practice. Multiple lumped capacitance models might be regarded as an intermediate step between a single lumped capacitance and a distributed capacitance. While the addition of more lumped capacitances might achieve a better fit to the data, it also requires a higher number of parameters to describe the system ($2n + 1$, where n is the number of lumped capacitances) resulting in a loss of simplicity and physical interpretability compared to distributed capacitance models.

When choosing the discrete time step considered for dynamic analysis, values around 1 h were found to be optimum for this wall. A finer resolution did not appear to improve predictions, and coarser sampling times (in the range of 6 to 24 h) caused non-convergence problems in the lumped capacitance method and unreliable estimates with the distributed capacitance method. These behaviours could be explained by the fading-out of transient effects in a timeframe of about 6 h (Fig. 9), so that sampling times above this figure would not adequately capture dynamic effects.

The monthly analysis also revealed interesting variations on parameter estimates (Fig. 11). Concretes A and C yielded similar estimates on their thermal resistance and capacitance along the whole experimental campaign. In contrast, towards the end of the campaign thermal resistance appeared to slightly decrease for concrete B, while it would have increased for concrete D. The three models studied agree on this behaviour, hinting at the assumption of time-invariant thermal properties not holding in this case. It is known that thermal conductivity is dependent on both temperature and moisture content [72], with a higher influence from the latter for concretes in usual building exposure conditions [73]. The replacement of water with air in the pores leads to a lower overall heat capacity and thermal resistance, and vice versa. Thermal capacitance estimates from the distributed capacitance method seem to confirm this reciprocal relation: August estimates of C increase for concrete B and decrease for concrete D. Parameter variations might therefore be attributed to real physical changes in the moisture content of the samples. This highlights the importance of *in situ* thermal performance tests (to complement lab measurements) covering a variety of exposure conditions.

Gori and Elwell [49] investigated the propagation of systematic measurement errors on thermal resistance estimates for a steady-state and a lumped capacitance model. They found the relative error to be dependent on the temperature difference between internal and external exposure conditions. For steady-state models (average method) the systematic measurement error was highly amplified for low temperature differences, to the extent of rendering the obtained estimates unreliable. Dynamic lumped capacitance methods led to lower systematic errors in all cases, and especially for low temperature differences, suggesting that these would allow measurements to be performed outside winter conditions and/or without the need of continuous space heating. Models with two lumped capacitances led to more consistent estimates of thermal resistance than those with a single lumped capacitance. It would be interesting to extend the formulation and application of analogous error propagation methods to heat capacitance estimates and to the distributed capacitance model proposed in the present study.

When drawing general conclusions from this study, it should be noted that the assessed wall has a particular configuration, consisting of a single quasi-homogeneous layer with no insulation. Building walls built in Europe in the last 40 years, and especially in recent times, are likely to include at least some thermal insulation. Precisely, the high thermal conductance (low R value) might explain why inertial effects are so short-lived (Fig. 9) despite the massive character (high C value) of the wall. It can be drawn from the horizontal axis of Fig. 5 that the duration of the transient response is a function of the product of thermal capacitance and resistance CR, which would be much longer in the presence of thermal insulation. Hence, optimum time steps for analysis and required campaign durations would depend not only on exposure conditions but also on wall characteristics, and particularly, on their thermal insulation values. A replication study on a well-insulated wall would thus provide a useful counterpoint to this work.

6. Conclusions

The *in situ* thermal performance of four uninsulated concrete panels of different formulation was monitored from December 2017 to August 2018. Three different methods were used for the characterisation of thermal performance, ranging from more widespread to more novel: (1) the average method in ISO 9869–1 [6] based on a steady-state model, (2) a stochastic method based on a resistance–capacitance (RC) lumped capacitance model, and (3) an analytical method based on a distributed capacitance model. The lumped and distributed capacitance models were chosen for their superior physical interpretation over data-driven dynamic methods. An analysis was performed for the influence of exposure conditions, time steps and campaign lengths on thermal resistance and capacitance estimations.

If the ultimate aim is the estimation of thermal resistance (and thus long-term cumulated heat flow through the walls), optimum test conditions are those that maximise heat flux by maintaining a steady difference between indoor and outdoor temperatures. For strong temperature differences (e.g. over 10 °C), simple steady-state models provided suitable results in a timeframe of 72 h (the minimum required by [6]). When the temperature difference was moderate (in the range of 5 °C) or included shifts in the direction of heat flow, lumped capacitance models provided reliable results without the need of extending campaign lengths over 72 h. If characterisation of thermal capacity is also sought (for predicting dynamic short-term response of the walls), optimum test conditions are those where both indoor and outdoor temperatures fluctuate. The steady-state method is unsuitable for this purpose since it does not give any indication of thermal capacity. Capacitance estimates obtained from lumped models were dependent on the specific data subset and the time step selected from analysis, and might not be extrapolated to exposure conditions that differ from the training data. Findings from this study suggest that a distributed capacitance model can provide physically consistent estimates for both thermal resistance and thermal capacitance.

The particularities and limitations of this study comprise the simplicity and prior knowledge of the wall assembly, as well as a long measurement campaign covering a wide range of indoor and outdoor conditions over different seasons. While the assumption of a single homogeneous layer allows the successful application of a distributed capacitance method, most wall assemblies have a more complex configuration, including layers of different thermal mass and insulation characteristics. Future research might investigate the extension of the analytical distributed capacitance method presented in this study to multi-layer walls with or without thermal insulation.

Declaration of Competing Interest

The authors declare that they have no known competing financial interests or personal relationships that could have appeared to influence the work reported in this paper.

Data availability

Data will be made available on request.

Acknowledgments

The experimental campaign featured in this study has received funding from the European Union's Horizon 2020 research and innovation programme under grant agreement ID 637138. This paper reflects only the authors' views and neither the Agency nor the Commission are responsible for any use that may be made of the information contained therein.

References

[1] United Nations, Global Status report for Buildings and Construction 2021, Nairobi, 2021. https://globalabc.org/resources/publications/2021-global-status-report-buildings-and-construction.
[2] European Union, Directive 2010/31/EU of the European parliament and of the Council of 19 May 2010 on the energy performance of buildings (recast), 2010.
[3] I. Nardi, S. Perilli, T. de Rubeis, S. Sfarra, D. Ambrosini, Influence of insulation defects on the thermal performance of walls, J. Build. Eng. 21 (2019) 355–365, https://doi.org/10.1016/j.jobe.2018.10.029.
[4] E. Cuerda, O. Guerra-Santin, J.J. Sendra, F.J. Neila, Understanding the performance gap in energy retrofitting: Measured input data for adjusting building simulation models, Energy Build. 209 (2020) (109688). https://doi.org/10.1016/j.enbuild.2019.109688.
[5] E. Mantesi, C.J. Hopfe, M.J. Cook, J. Glass, P.A. Strachan, The modelling gap: Quantifying the discrepancy in the representation of thermal mass in building simulation, Build. Environ. 131 (2018) 74–98, https://doi.org/10.1016/j.buildenv.2017.12.017.
[6] ISO, ISO 9869-1:2014 Thermal insulation – Building elements – In-situ measurement of thermal resistance and thermal transmittance – Part 1: Heat flow meter method, ISO. (2014).
[7] Y. Yang, Z. Chen, T. Vogt, A. Sempey, J. Batsale, In situ methodology for thermal performance evaluation of building wall: a review, Int. J. Therm. Sci. (2022) (107687), https://doi.org/10.1016/j.ijthermalsci.2022.107687.
[8] D. Bienvenido-Huertas, J.J. Moyano, D. Marín, R. Fresco-Contreras, Review of in situ methods for assessing the thermal transmittance of walls, Renew. Sustain. Energy Rev. 102 (2019) 356–371, https://doi.org/10.1016/j.rser.2018.12.016.
[9] M. Teni, H. Krstić, P. Kosiński, Review and comparison of current experimental approaches for in-situ measurements of building walls thermal transmittance, Energy Build. 203 (2019) (109417). https://doi.org/10.1016/j.enbuild.2019.109417.
[10] X.-F. Zhu, L.-P. Li, X.-B. Yin, S.-H. Zhang, Y. Wang, W. Lui, L. Zheng, An in-situ test apparatus of heat transfer coefficient for building envelope, Build. Energy Effic. 256 (2012) 57–60.
[11] X. Meng, T. Luo, Y. Gao, L. Zhang, Q. Shen, E. Long, A new simple method to measure wall thermal transmittance in situ and its adaptability analysis, Appl. Therm. Eng. 122 (2017) 747–757, https://doi.org/10.1016/j.applthermaleng.2017.05.074.
[12] J. Meulemans, F. Alzetto, D. Farmer, C. Gorse, QUB/e: A novel transient experimental method for in situ measurements of the thermal performance of building fabrics, in: Build. Inf. Model. Build. Performance, Des. Smart Constr., 2017: pp. 115–127. https://doi.org/10.1007/978-3-319-50346-2.
[13] A. François, L. Ibos, V. Feuillet, J. Meulemans, Estimation of the thermal resistance of a building wall with inverse techniques based on rapid active in situ measurements and white-box or ARX black-box models, Energy Build. 226 (2020) 110346.
[14] A. Rasooli, L. Itard, C. Infante Ferreira, A response factor-based method for the rapid in-situ determination of wall's thermal resistance in existing buildings, Energy Build. 119 (2016) 51–61, https://doi.org/10.1016/j.enbuild.2016.03.009.
[15] H. Melgaard, Identification of physical models, 1994. http://orbit.dtu.dk/fedora/objects/orbit:78530/datastreams/file_2833556/content.
[16] K. Martin, I. Flores, C. Escudero, A. Apaolaza, J.M. Sala, Methodology for the calculation of response factors through experimental tests and validation with

simulation, Energy Build. 42 (2010) 461–467, https://doi.org/10.1016/j.enbuild.2009.10.015.
[17] S. Wang, Y. Chen, A simple procedure for calculating thermal response factors and conduction transfer functions of multilayer walls, Appl. Therm. Eng. 22 (2002) 333–338, https://doi.org/10.1016/S1359-4311(01)00086-2.
[18] I. Naveros, C. Ghiaus, D.P. Ruiz, S. Castaño, Physical parameters identification of walls using ARX models obtained by deduction, Energy Build. 108 (2015) 317–329, https://doi.org/10.1016/j.enbuild.2015.09.021.
[19] M.J. Jiménez, H. Madsen, K.K. Andersen, Identification of the main thermal characteristics of building components using MATLAB, Build. Environ. 43 (2008) 170–180, https://doi.org/10.1016/j.buildenv.2006.10.030.
[20] D. Bienvenido-Huertas, C. Rubio-Bellido, J.L. Pérez-Ordóñez, M.J. Oliveira, Automation and optimization of in-situ assessment of wall thermal transmittance using a Random Forest algorithm, Build. Environ. 168 (2020) (106749), https://doi.org/10.1016/j.buildenv.2019.106479.
[21] R. Baccoli, L. Di Pilla, A. Frattolillo, C.C. Mastino, An adaptive neural network model for thermal characterization of building components, Energy Procedia 140 (2017) 374–385, https://doi.org/10.1016/j.egypro.2017.11.150.
[22] D. Bienvenido-Huertas, J. Moyano, C.E. Rodríguez-Jiménez, D. Marín, Applying an artificial neural network to assess thermal transmittance in walls by means of the thermometric method, Appl. Energy. 233–234 (2019) 1–14, https://doi.org/10.1016/j.apenergy.2018.10.052.
[23] J. Vivian, A. Zarrella, G. Emmi, M. De Carli, An evaluation of the suitability of lumped-capacitance models in calculating energy needs and thermal behaviour of buildings, Energy Build. 150 (2017) 447–465, https://doi.org/10.1016/j.enbuild.2017.06.021.
[24] Z. Wang, Y. Chen, Y. Li, Development of RC model for thermal dynamic analysis of buildings through model structure simplification, Energy Build. 195 (2019) 51–67, https://doi.org/10.1016/j.enbuild.2019.04.042.
[25] Y. Li, Z. O'Neill, L. Zhang, J. Chen, P. Im, J. DeGraw, Grey-box modeling and application for building energy simulations - a critical review ☆, Renew. Sustain. Energy Rev. 146 (2021) (111174), https://doi.org/10.1016/j.rser.2021.111174.
[26] O.M. Brastein, B. Lie, R. Sharma, N.-O. Skeie, Parameter estimation for externally simulated thermal network models, Energy Build. 191 (2019) 200–210, https://doi.org/10.1016/j.enbuild.2019.03.018.
[27] I. Naveros, P. Bacher, D.P. Ruiz, M.J. Jiménez, H. Madsen, Setting up and validating a complex model for a simple homogeneous wall, Energy Build. 70 (2014) 303–317, https://doi.org/10.1016/j.enbuild.2013.11.076.
[28] A.P. Ramallo-González, M.E. Eames, D.A. Coley, Lumped parameter models for building thermal modelling: an analytic approach to simplifying complex multi-layered constructions, Energy Build. 60 (2013) 174–184, https://doi.org/10.1016/j.enbuild.2013.01.014.
[29] V. Gori, P. Biddulph, C.A. Elwell, A Bayesian dynamic method to estimate the thermophysical properties of building elements in all seasons, orientations and with reduced error, Energies 11 (2018) (802), https://doi.org/10.3390/en11040802.
[30] C.P. Underwood, F.W.H. Yik, Modelling methods for energy in buildings, Blackwell (2004), https://doi.org/10.1002/9780470758533.
[31] O. Gutschker, Parameter identification with the software package LORD, Build. Environ. 43 (2008) 163–169, https://doi.org/10.1016/j.buildenv.2006.10.010.
[32] X. Yu, L. Georges, L. Imsland, Data pre-processing and optimization techniques for stochastic and deterministic low-order grey-box models of residential buildings, Energy Build. 236 (2021) (110775), https://doi.org/10.1016/j.enbuild.2021.110775.
[33] ISO, ISO 13786 Thermal performance of building components – Dynamic thermal characteristics – Calculation methods, ISO. (2019). https://doi.org/10.1017/CBO9781107415324.004.
[34] K. Ulgen, Experimental and theoretical investigation of effects of wall's thermophysical properties on time lag and decrement factor, Energy Build. 34 (2002) 273–278, https://doi.org/10.1016/S0378-7788(01)00087-1.
[35] C. Luo, B. Moghtaderi, S. Hands, A. Page, Determining the thermal capacitance, conductivity and the convective heat transfer coefficient of a brick wall by annually monitored temperatures and total heat fluxes, Energy Build. 43 (2011) 379–385, https://doi.org/10.1016/j.enbuild.2010.09.030.
[36] M. Faye, B. Lartigue, V. Sambou, A new procedure for the experimental measurement of the effective heat capacity of wall elements, Energy Build. 103 (2015) 62–69, https://doi.org/10.1016/j.enbuild.2015.05.054.
[37] C. Balocco, V. Gori, E. Marmonti, L. Citi, Building-plant system energy sustainability. An approach for transient thermal performance analysis, Energy Build. 49 (2012) 443–453, https://doi.org/10.1016/j.enbuild.2012.02.048.
[38] R.G. Martinez, A. Riverola, D. Chemisana, Disaggregation process for dynamic multidimensional heat flux in building simulation, Energy Build. 148 (2017) 298–310, https://doi.org/10.1016/j.enbuild.2017.05.029.
[39] M.G. Davies, Building heat transfer, Wiley (2004), https://doi.org/10.1002/0470020555.
[40] J. Berger, S. Gasparin, D. Dutykh, N. Mendes, On the comparison of three numerical methods applied to building simulation: finite-differences, RC circuit approximation and a spectral method, Build. Simul. 13 (2020) 1–18, https://doi.org/10.1007/s12273-019-0555-z.
[41] M. Cucumo, A. De Rosa, V. Ferraro, D. Kaliakatsos, V. Marinelli, A method for the experimental evaluation in situ of the wall conductance, Energy Build. 38 (2006) 238–244, https://doi.org/10.1016/j.enbuild.2005.06.005.
[42] L. Evangelisti, C. Guattari, P. Gori, F. Asdrubali, Assessment of equivalent thermal properties of multilayer building walls coupling simulations and experimental measurements, Build. Environ. 127 (2018) 77–85, https://doi.org/10.1016/j.buildenv.2017.10.038.
[43] A. Rodler, S. Guernouti, M. Musy, Bayesian inference method for in situ thermal conductivity and heat capacity identification: Comparison to ISO standard, Constr. Build. Mater. 196 (2019) 574–593, https://doi.org/10.1016/j.conbuildmat.2018.11.110.
[44] T. Šuklje, M. Hamdy, C. Arkar, J.L.M. Hensen, S. Medved, An inverse modeling approach for the thermal response modeling of green façades, Appl. Energy. 235 (2019) 1447–1456, https://doi.org/10.1016/j.apenergy.2018.11.066.
[45] ECO-BINDER, Development of insulating concrete systems based on novel low CO2 binders for a new family of eco-innovative, durable and standardized energy efficient envelope components, (n.d.). https://cordis.europa.eu/project/id/637138 (accessed July 28, 2022).
[46] R. Garay, J.A. Chica, I. Apraiz, J.M. Campos, B. Tellado, A. Uriarte, V. Sanchez, Energy efficiency achievements in 5 years through experimental research in KUBIK, Energy Procedia 78 (2015) 865–870, https://doi.org/10.1016/j.egypro.2015.11.009.
[47] R. San Mateos Carretón, R. Garay-Martinez, Z. Eguiluz, Experimentation of new products and solutions at full scale in Kubik. Its evolution and transformation in 10 years of operation, Rehabend, in, 2022.
[48] M. Kottek, J. Grieser, C. Beck, B. Rudolf, F. Rubel, World map of the Köppen-Geiger climate classification updated, Meteorol. Zeitschrift. 15 (3) (2006) 259–263.
[49] V. Gori, C.A. Elwell, Estimation of thermophysical properties from in-situ measurements in all seasons: quantifying and reducing errors using dynamic grey-box methods, Energy Build. 167 (2018) 290–300, https://doi.org/10.1016/j.enbuild.2018.02.048.
[50] K. Gaspar, M. Casals, M. Gangolells, Review of criteria for determining HFM minimum test duration, Energy Build. 176 (2018) 360–370, https://doi.org/10.1016/j.enbuild.2018.07.049.
[51] I.A. Atsonios, I.D. Mandilaras, D.A. Kontogeorgos, M.A. Founti, A comparative assessment of the standardized methods for the in–situ measurement of the thermal resistance of building walls, Energy Build. 154 (2017) 198–206, https://doi.org/10.1016/j.enbuild.2017.08.064.
[52] P.E. Bagnoli, C. Casarosa, M. Ciampi, E. Dallago, Thermal resistance analysis by induced transient (TRAIT) method for power electronic devices thermal characterization - Part I: fundamentals and theory, IEEE Trans. Power Electron. 13 (1998) 1208–1219.
[53] H. Madsen, P. Bacher, P. Delff, Mathematical and statistical models and methods for describing the thermal characteristics of buildings. DYNASTEE Int. Work. Dyn. Methods Build, Energy Assessment, Brussels, 2010.
[54] G. Masy, Definition and validation of a simplified multizone dynamic building model connected to heating system and HVAC unit, Université de Liège, 2008.
[55] R. Juhl, J.K. Møller, H. Madsen, ctsmr – Continuous Time Stochastic Modeling in R, ArXiv. (2016). https://doi.org/10.48550/ARXIV.1606.00242.
[56] G. Anderlind, Dynamic Thermal Models: Two dynamic models for estimating thermal resistance and heat capacity from in situ measurements, 1996.
[57] D. Maillet, S. André, J.C. Batsale, A. Degiovanni, C. Moyne, Thermal Quadrupoles: Solving the heat equation through integral transforms, (2000).
[58] U. Norlén, Determining the thermal resistance from in-situ measurements, in: Work. Appl. Syst. Identif. Energy Savings Build., 1994: pp. 402–429.
[59] G. James, D. Witten, T. Hastie, R. Tibshirani, An Introduction to Statistical Learning with Applications in R (2013), https://doi.org/10.1007/978-1-4614-7138-7.
[60] A. Rasooli, In-situ -determination of buildings' thermo-physical characteristics, TU Delft, 2020.
[61] E. Biteau, D. Defer, F. Brachelet, L. Zalewski, Active thermal method applied to the in situ characterization of insulating materials in a wall, Buildings 11 (2021) 578, https://doi.org/10.3390/buildings11120578.
[62] R. O'Hegarty, O. Kinnane, S.J. McCormack, Parametric investigation of concrete solar collectors for façade integration, Sol. Energy. 153 (2017) 396–413, https://doi.org/10.1016/j.solener.2017.05.092.
[63] H.R. Talebi, B.A. Kayan, I. Asadi, Z.F.B.A. Hassan, Investigation of thermal properties of normal weight concrete for different strength classes, J. Environ. Treat. Tech. 8 (2020) 908–914.
[64] P. Shafigh, I. Asadi, N.B. Mahyuddin, Concrete as a thermal mass material for building applications - a review, J. Build. Eng. 19 (2018) 14–25, https://doi.org/10.1016/j.jobe.2018.04.021.
[65] T.L. Cavalline, R.W. Castrodale, C. Freeman, J. Wall, Impact of lightweight aggregate on concrete thermal properties, ACI Mater. J. 114 (2017) 945–956, https://doi.org/10.14359/51701003.
[66] K. Gaspar, M. Casals, M. Gangolells, A comparison of standardized calculation methods for in situ measurements of façades U-value, Energy Build. 130 (2016) 592–599, https://doi.org/10.1016/j.enbuild.2016.08.072.
[67] B. Arregi, R. Garay-Martinez, J. Astudillo, J.C. Ramos, J. Kurnitski, T. Kalamees, Monitoring and thermal performance evaluation of two building envelope solutions in an apartment building, E3S Web Conf. 172 (2020) 25002.
[68] P. Biddulph, V. Gori, C.A. Elwell, C. Scott, C. Rye, R. Lowe, T. Oreszczyn, Inferring the thermal resistance and effective thermal mass of a wall using frequent temperature and heat flux measurements, Energy Build. 78 (2014) 10–16, https://doi.org/10.1016/j.enbuild.2014.04.004.
[69] P. Gori, L. Evangelisti, C. Guattari, Description of multilayer walls by means of equivalent homogeneous models, Int. Commun. Heat Mass Transf. 91 (2018) 30–39, https://doi.org/10.1016/j.icheatmasstransfer.2017.11.008.
[70] V. Gori, V. Marincioni, P. Biddulph, C.A. Elwell, Inferring the thermal resistance and effective thermal mass distribution of a wall from in situ measurements to characterise heat transfer at both the interior and exterior surfaces, Energy Build. 135 (2017) 398–409, https://doi.org/10.1016/j.enbuild.2016.10.043.

[71] X. Xu, S. Wang, Optimal simplified thermal models of building envelope based on frequency domain regression using genetic algorithm, Energy Build. 39 (2007) 525–536, https://doi.org/10.1016/j.enbuild.2006.06.010.
[72] L.D. Hung Anh, Z. Pásztory, An overview of factors influencing thermal conductivity of building insulation materials, J. Build. Eng. 44 (2021) (102604), https://doi.org/10.1016/j.jobe.2021.102604.
[73] Y. Wang, C. Ma, Y. Liu, D. Wang, J. Liu, Effect of moisture migration and phase change on effective thermal conductivity of porous building materials, Int. J. Heat Mass Transf. 125 (2018) 330–342, https://doi.org/10.1016/j.ijheatmasstransfer.2018.04.062.